To cite this article: HE W, GUO J W, HU X F, et al. Influence of lift distribution coefficient on hydrodynamic performance of propeller in forward and astern mode of operation by numerical analysis [J/OL]. Chinese Journal of Ship Research, 2022, 17(1). http://www.ship-research.com/en/article/doi/10.19693/j.issn.1673-3185.02288.

DOI: 10.19693/j.issn.1673-3185. 02288

Influence of lift distribution coefficient on hydrodynamic performance of propellers in forward and astern operation modes by numerical analysis

HE Wei[1], *GUO Jiawei*[1], *HU Xiaofei*[2], *Liu Mingjing*[2], *BAI Tiechao*[2], *LI Ziru**[1]

1 School of Naval Architecture, Ocean and Energy Power Engineering, Wuhan University of Technology, Wuhan 430063, China

2 China Ship Development and Design Center, Wuhan 430064, China

Abstract: [**Objectives**] The influence of the geometrical parameters of a propeller on its hydrodynamic performance in the forward and astern modes of operation is studied by numerical simulation. [**Methods**] Taking a 33 000 DWT oil product tanker as the application object, we simulate the hydrodynamic performance of an MAU-series propeller and three theoretical propellers operated in forward and astern modes using the RANS method combined with the Realizable k-ε turbulence model. The influence of the lift distribution coefficient, as well as the pitch and camber combinations, on the hydrodynamic performance of the propeller in both operation modes are then discussed through comparison. [**Results**] The results reveal that in forward and astern operation modes, the pitch of the blade sections will generate positive lift, whereas the camber of the blade sections will produce positive and negative lift alternately. Properly increasing the camber and reducing the pitch of the propeller in design is beneficial for improving its open water efficiency in the forward operation mode while adopting the combination of a large pitch and a small camber is beneficial for increasing reverse thrust. [**Conclusion**] On the basis of the experimental data, suggestions on performance trade-offs of designing a propeller in both operation modes are given.

Key words: propeller performance; astern operation; forward operation; hydrodynamic performance; RANS

CLC number: U661.31

0 Introduction

Most of the research on the influence of the geometrical parameters of a ship propeller on its hydrodynamic performance only focuses on the forward operation mode (i.e., turning ahead while going forward in this study) of the propeller, and the discussion on the astern operation mode (i. e., turning astern while going backward in this study) is scarce. In the related research on the design method and engineering application of the propeller, the astern performance of the propeller is seldom used as the design goal or evaluation index, and the discussion on the influence of geometrical parameters of the propeller on the reverse thrust is rare. In the process of geometry design of the propeller, the related design and engineering experience of how to effectively increase the reverse thrust or consider

Received: 2021－02－02 **Accepted**: 2021－04－07

Supported by: National Natural Science Foundation of China (51609189); Fundamental Research Funds for the Central Universities (2019III076GX)

Authors: HE Wei, male, born in 1982, Ph.D., associate professor. Research interest: ship propulsion hydrodynamics.
E-mail: hwcudca@163.com
GUO Jiawei, male, born in1997, master degree candidate. Research interest: ship propulsion technology.
E-mail: 253418533@qq.com
LI Ziru, female, born in 1983, Ph.D., associate professor. Research interest: ship hydrodynamics.
E-mail: lisay333@163.com

***Corresponding author**: LI Ziru

the performance trade-offs in forward and astern operation modes is particularly lacking.

In the study on the hydrodynamic performance of the propeller in a non-forward operation mode, Hecker et al. [1] used experiments to predict the hydrodynamic performance of eight propeller models with different geometrical shapes in four quadrants (forward, emergency stop, emergency start, and astern). It was found that the hydrodynamic characteristic curve of the propeller would present inflection points under medium load conditions in an emergency stop and emergency start. JIANG et al. [2] proposed a method for predicting the hydrodynamic performance of propellers in emergency stop and astern operation modes by using the panel method, focusing on improving the realization of the Kutta condition in special operation modes. On the basis of the panel method, WANG [3] predicted the variation laws of thrust, torque, efficiency, and rotor torque with the pitch angle of the JDC7704 controllable pitch propeller in multiple operation modes from the astern to the forward. By the RANS method, LAI [4] calculated the hydrodynamic performance of an MAU-series propeller in forward and astern operation modes and pointed out that the thrust coefficient, torque coefficient, and open water efficiency of the propeller in the astern operation mode all decreased compared with those in the forward operation mode. CHEN et al. [5-6], LEE [7], XIAO et al. [8], and LI et al. [9] predicted the hydrodynamic performance of propellers in four quadrants by combining the RANS method with the Chimera moving grid approach, overset grid approach, method of rotating coordinate frame (MRF), and sliding grid method, respectively. It was found that the flow field of the propeller is relatively smooth in the first and fourth quadrants, and the MRF method can be used. However, it is nonlinear in the second and third quadrants, and different numerical solutions are required to accurately simulate the flow field, such as the sliding grid method, moving grid method, or the overset grid method. WANG et al. [10] used the same method to expand the research object to the ducted propeller. WANG [11] took the DTMB438X-series propellers as the research object and discussed the influence of blade skew on the hydrodynamic performance in the non-forward operation modes by the RANS method. The results indicated that blade skew has no significant effect on the performance under forward and emergency stop operation modes, but it would largely degrade the open water performance of the medium load area (J = 0.5 – 0.8) in the astern operation mode. YANG et al. [12] used similar methods and came to the same conclusion. The above studies all show that the RANS method can accurately predict the hydrodynamic performance of propellers in four quadrants, but almost all of them only focus on the variation laws of the hydrodynamic performance of a propeller with a given geometrical shape with the operation modes, and the discussion on the influence of geometrical parameters on the astern performance of the propeller is insufficient.

The original sister ship of a 33 000 DWT oil product tanker discussed in this paper adopts an MAU-series propeller. To improve the comprehensive navigation performance of the new ship, the MAU-series propeller is replaced by a propeller based on circulation theory with medium skew. During the sea trial, its maximum speed and vibration have certain advantages over its original sister ship, but its low-speed astern performance is lower. At the same speed, the reverse thrust of the theoretical propeller of the new ship is lower than that of the MAU-series propeller of the original ship. Therefore, this paper will use the CFD method to study this phenomenon to explain the reason why the reverse thrust of the theoretical propeller is lower than that of the MAU-series propeller. Firstly, by the design method of circulation theory, it is required that the thrust of the propeller in the designed forward operation mode is equivalent to that of the original theoretical propeller, and the lift distribution coefficient is reduced in turn to design another two theoretical propellers with zero camber and negative camber. Then, by comparing numerical results of the hydrodynamic performance of four propellers in forward and astern operation modes, the influence of the lift distribution coefficient and the pitch and camber combinations on the hydrodynamic performance of propellers in both operation modes is discussed. It is expected that this research can thereby provide some reference for performance trade-offs of designing a propeller in both operation modes.

1 Research object

The design parameters of the 33 000 DWT oil product tanker and its propellers are shown in Table 1, and the view of the ship is shown in Fig. 1. The two ships adopt the MAU-series propeller and the theoretical propeller, respectively. For the convenience of narration, the two propellers are denoted as the MAU-series propeller and theoretical propeller 1, and their main parameters are listed in Table 2. Figs. 2 and 3 show the geometry of the two propellers and their distributions of the pitch ratio P/D and the camber-chord length ratio F/C along the radial direction r/R, respectively.

Table 1 Design parameters of ship and propellers

Parameter	Value
Ship length/m	175.0
Block coefficient	0.813
Design speed/kn	13.0
Main engine power/kW	6 340
Power reservation coefficient	0.15
Shafting efficiency	0.97
Wake fraction	0.270
Thrust deduction fraction	0.155
Relative rotative efficiency	0.985
Propeller speed/(r·min^{-1})	136

Fig. 1 View of 33 000 DWT oil product tanker

Table 2 Main geometric parameters of MAU-series propeller and theoretical propeller 1

Parameter	Value	
	MAU-series propeller	Theoretical propeller 1
Propeller diameter/m	5	5
Number of blades	5	5
Disk ratio	0.55	0.55
Hub diameter ratio	0.18	0.18
Pitch ratio at 0.7R	0.700 0	0.748 6
Skew angle/(°)	10	24.5
Section type	MAU	NACA66

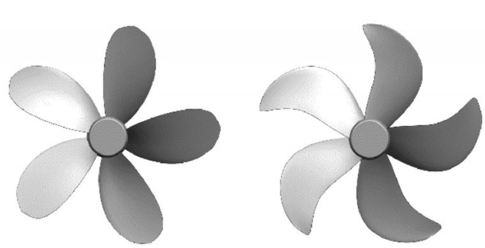

(a) MAU-series propeller (b) Theoretical propeller 1

Fig. 2 Geometry of two propellers

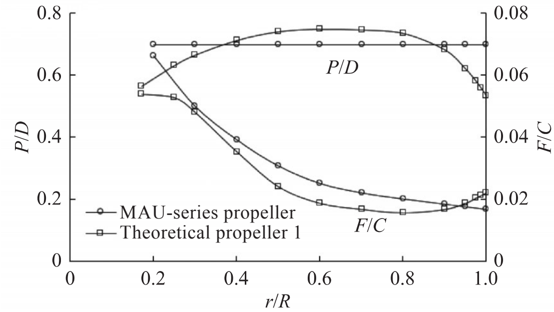

Fig. 3 Radial distribution of pitch ratio and camber-chord length ratio of two propellers

Before the follow-up study, the following points need to be explained.

1) The design of the new ship propeller adopts the circulation theory, which will not be introduced in this paper due to space limitations, but the details can be found in Ref. [13]. In the design of theoretical propellers, the best circulation distribution form is selected, and for the theoretical propeller 1, the lift distribution coefficient C_F of blade sections is taken as 0.7 at the radius, where C_F is the ratio of the zero-lift angle of attack to the absolute angle of attack of blade sections, reflecting the contribution of the sectional camber to the lift.

2) To facilitate the comparison with experimental results of the model and reduce the workload of numerical calculations, the numerical calculations in this paper are based on the scale of the model. The contracting ratio is 25, namely that the diameter D of the propeller model is 200 mm, and the speed n of the propeller model is 2 000 r/min according to the critical Reynolds number.

3) Although the speed of the new ship and its original sister ship equipped with different propellers all exceed the design speed of 13 kn, the actual speed is slightly different due to different propeller efficiency, and the actual balance state of the ship-engine-propeller linkage of the two ships is not the same. To reduce the complexity caused by inconsistent matching points, the speed is unified to 13 kn when discussing the forward operation mode, and the corresponding advance coefficient J equals 0.430 8. In the subsequent theoretical propeller design, the constraint is that the propeller thrust is equivalent to that of the original theoretical propeller in this operation mode.

4) For the astern operation mode, given the possible influence of the speed limit of the main engine, the professional level and habits of the ship operator, the ship attitude, and the water flow conditions on the astern condition, this paper assumes that the

ship moves back at relatively low speed with the propeller rotating backward when discussing the astern performance of the propeller, and the calculation and comparison are carried out only for the astern open water operation mode with the corresponding advance coefficient J of 0−0.1.

2 Numerical model and validation

In this paper, the CFD method is used to predict and compare the hydrodynamic performance of the propeller in forward and astern operation modes. The adopted numerical model is outlined below.

2.1 Governing equation

The governing equation of viscous flow around the propeller is Navier-Stokes (N-S) equation, and the continuity equation and momentum conservation equation after time averaging are given by

$$\frac{\partial \bar{u}_i}{\partial x_i} = 0, \quad i = 1,2,3 \tag{1}$$

$$\frac{\partial \bar{u}_i}{\partial t} + \bar{u}_j \frac{\partial \bar{u}_i}{\partial x_j} = -\frac{1}{\rho}\frac{\partial \bar{p}}{\partial x_i} + \frac{\mu}{\rho}\nabla \cdot \nabla \bar{u}_i + \frac{1}{\rho}\frac{\partial\left(-\rho\overline{u_i' u_j'}\right)}{\partial x_i} \tag{2}$$

where x_i and x_j are the i-th and j-th components of the coordinate system, respectively, and j = 1, 2, and 3; $\bar{u}_i$ and $\bar{u}_j$ are the time average of the velocity components; $\bar{p}$ is the average pressure on the fluid element; μ is the kinematic viscosity coefficient; ρ is the water density; $-\rho\overline{u_i' u_j'}$ is the Reynolds stress; ∇ is the gradient operator.

2.2 Computational domain and grid division

The setting of the computational domain affects both the accuracy and efficiency of numerical calculations. Considering the advantages and disadvantages of an excessively large computational domain and by referring to Ref. [14], the selected computational domain is shown in Fig. 4, where the computational domain has two cylindrical regions coaxial with the propeller, i. e., the rotating inner domain and stationary outer domain surrounding the propeller. The propeller diameter is D; the diameter of the rotating domain is 1.2D, and its length is 1D. The diameter of the stationary domain is 8D, and its length is 13D. In view of the calculation requirement of the forward and astern operation modes, the geometrical centers of both the rotating domain and the stationary domain coincide with the center of the propeller. The propeller shaft is aligned with the X-axis of the coordinate system, and the direction pointing to the stern is positive. The Y-axis is positive upward, and the Z-axis follows the right-hand rule.

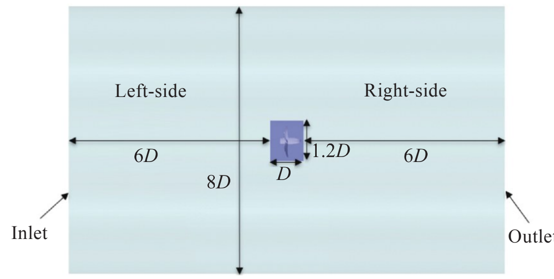

Fig. 4 Computational domain

The grid generator of the software STAR-CCM+ is used for the grid division of the computational domain. The grids of the rotating domain and stationary domain are divided by the cutter generator, and the boundary layer grids are divided by the grid generator of prismatic layers. In the rotating domain, the grid size of the blade and hub surface is set to 0.005D; the grid size of the body is set to 0.01D, and the grid size of the interface is set to 0.01D. The boundary layer grids are set on the near walls of the blade and hub. Through debugging, the wall Y^+ value is eventually controlled at about 100.

To facilitate the use of the same set of grids for subsequent numerical calculations of the hydrodynamic performance of the propeller in forward and astern operation modes, we refined the grids in both inflow and outflow directions of the propeller in the stationary domain as well as the cylindrical region with the same diameter in the rotating domain. Fig. 5 shows the grid diagram in the sections with X = 0 and Y = 0.

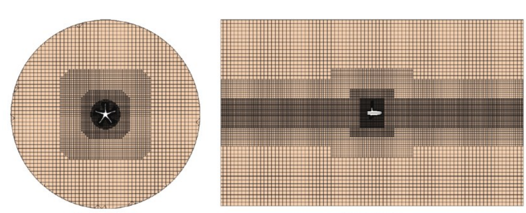

Fig. 5 Grid diagrams of feature sections in computational domain

2.3 Turbulence model and boundary conditions

By referring to the processing experience in Ref. [14] on numerical calculations of the hydrodynamic performance of the propeller in forward and astern operation modes, the boundary conditions of the computational domain and the rotational direction of the propeller are shown in Table 3. The inlet and outlet boundary conditions are set as the velocity inlet and the pressure outlet, respectively, and the relative pressure is 0 Pa. The MRF method is employed to simulate the rotation of the propeller, with the interface between the rotating domain and the stationary domain being Interface and the turbulence model being the Realizable k-ε model.

Table 3 Definition of rotational direction of propeller and boundary conditions of computational domain

Item	Forward	Astern
Inflow direction	X	$-X$
Rotational direction of the propeller	$-X$	X
Left-side boundary conditions of the computational domain	Velocity inlet	Pressure outlet
Right-side boundary conditions of the computational domain	Pressure outlet	Velocity inlet
Far-field boundary conditions	Symmetric plane	Symmetric plane
Boundary conditions of the blade and hub	Non-slip wall	Non-slip wall

2.4 Validation

For easy comparison, the hydrodynamic performance of the propeller is expressed in a dimensionless form. The propeller thrust coefficient K_T, torque coefficient K_Q, and open water efficiency η_0 are defined as

$$K_T = \frac{T}{\rho n^2 D^4} \tag{3}$$

$$K_Q = \frac{Q}{\rho n^2 D^5} \tag{4}$$

$$\eta_0 = \frac{J}{2\pi} \cdot \frac{K_T}{K_Q} \tag{5}$$

$$J = \frac{V_{\mathrm{A}}}{nD} \tag{6}$$

where T is the propeller thrust, N; Q is the propeller torque, N·m; n is the propeller speed, s^{-1}; D is the propeller diameter, m; ρ is the fluid density, kg/m^3; V_{A} is the advance velocity, m/s.

On the basis of the above numerical method, the numerical calculation model for the theoretical propeller 1 is first built, and the open water performance of the propeller in the forward operation mode when J = 0−0.635 5 is numerically calculated. In the model experiment, the size of the propeller model and its speed are the same as that in the numerical calculation, and the numerical calculations are compared with experimental results [15], as shown in Fig. 6. It can be seen that the relative error between them is small, which is within 5% in most operation modes, and this indicates the effectiveness of the numerical calculation model in predicting the hydrodynamic performance of the propeller.

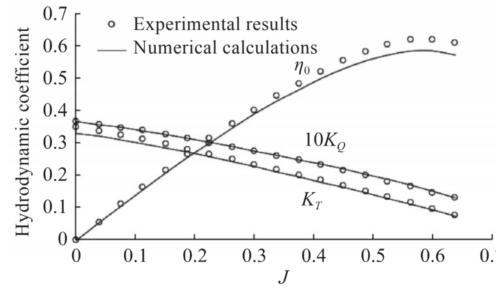

Fig. 6 Comparison of open water performance between numerical and experimental results of theoretical propeller 1

3 Comparison of hydrodynamic performance between MAU-series propeller and theoretical propeller 1

3.1 Forward operation mode

By the above numerical calculation model, the open water performance of the MAU-series propeller used by the original sister ship in the forward operation mode was also numerically calculated, and the comparison with that of the theoretical propeller 1 is shown in Fig. 7. In the forward operation mode with the design advance coefficient J of 0.430 8, the thrust coefficient and torque coefficient of the theoretical propeller 1 are reduced by 0.8% and 2.3%, and the open water efficiency is increased by 1.5%, compared with those of the MAU-series propeller. When J < 0.3, the thrust coefficient and torque coefficient of the theoretical propeller 1 are greater than those of the MAU-series propeller, and the increase in the thrust coefficient is significantly higher than that of the torque coefficient. When J < 0.55, the open water efficiency of the theoretical propeller 1 is higher than that of the MAU-series propeller, which is basically consistent with the trial results of the two ships.

Fig. 8 shows the pressure distribution of the two

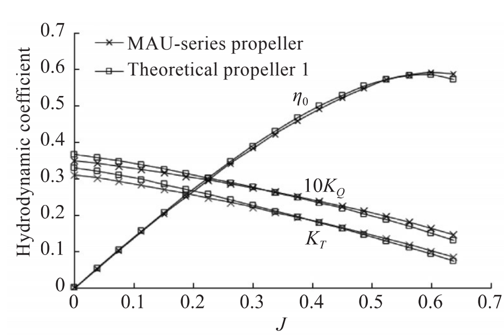

Fig. 7 Comparison of numerical calculations of two propellers in open water performance in forward operation mode

propellers in the forward operation mode with the design advance coefficient J being 0.430 8. In the blade tip area, the load of the MAU-series propeller is significantly higher than that of the theoretical propeller 1, while the load of the theoretical propeller 1 is slightly higher at the middle radius position, which is basically consistent with the radial distribution characteristics of the pitch and camber of the two propellers given in Fig. 3.

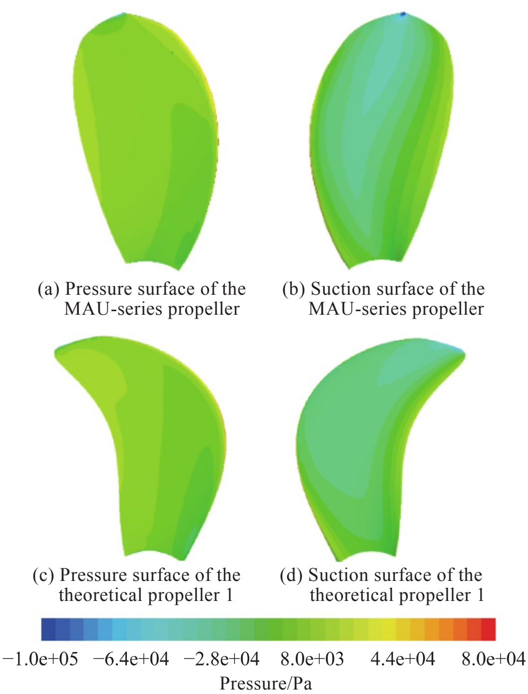

Fig. 8 Pressure distribution on blades of the two propellers in forward operation mode with J = 0.430 8

3.2 Astern operation mode

Fig. 9 shows the comparison results in the hydrodynamic performance of the two propellers in the astern operation mode when J = 0 – 0.1. It can be seen that the load of the two propellers decreases gradually with the increase in the advance coefficient, which conforms to that given in other references. The load of the theoretical propeller 1 in the astern operation mode is significantly lower than that of the MAU-series propeller. When J = 0, the thrust coefficient and torque coefficient of the theoretical propeller 1 are about 95.8% and 93.6% of that of the MAU-series propeller, respectively, and the deviation between the two has a gradually increasing trend with the increase in the advance coefficient. In other words, at the same reverse speed of the corresponding two real propellers, the reverse thrust generated by the MAU-series propeller is indeed greater than that of the theoretical propeller 1, and the ship's astern response is faster. The result is consistent with the relationship between the reverse thrust of the two ships in actual navigation.

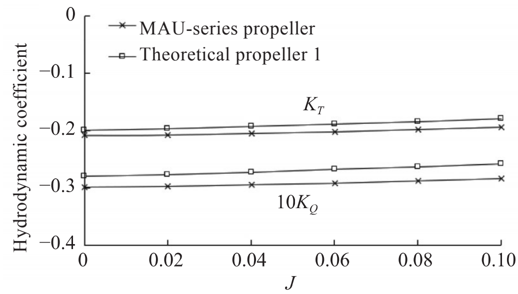

Fig. 9 Comparison of numerical results of two propellers in open water performance in astern operation mode

To explain the reasons for the difference in the hydrodynamic performance of the two propellers in the astern operation mode, we take the astern operation mode with J = 0.1 as an example, and Fig. 10 shows the comparison of the pressure distribution of the two propeller blades. Compared with the forward operation mode, the blade rotates reversely in the astern operation mode, and the positions of the blade's leading edge and trailing edge, as well as the positions of the suction surface and pressure surface, are exchanged. The figure indicates that although the peak pressure of the theoretical propeller 1 is slightly higher at the leading edge, both the area of high pressure on the pressure surface and the area of low pressure on the suction surface are smaller than those of the corresponding areas of the MAU-series propeller, especially in the blade tip area of the suction surface. On the one hand, this result reflects the influence of different radial load distributions of the two propellers; on the other hand, it reflects the influence of different blade sections of the two propellers. In contrast with the equal pitch characteristics of the MAU-series propeller, the theoretical propeller 1 is unloaded to a certain extent in both the root and tip of the blade where the pitch ratio is relatively small, and the load is low. Furthermore, the blade sections of the theoretical propeller 1 at each radius are wing-shaped, and the characteristic of a thick leading edge and a thin trailing edge is obvious. However, the blade sections of the MAU-series propeller at the outer radius area are bow-shaped, and the geometry of the leading edge and the trailing edge is close. Therefore, on the whole, it shows that loads of the MAU-series propeller in both operation modes are close while the astern load of the theoretical propeller 1 is significantly lower than its forward load.

Fig. 10 also demonstrates that the propeller in the astern operation mode has the largest pressure difference between the blade back and the blade face at the thinnest leading edge of the blade tip, especially for the theoretical propeller 1 with medium skew. The blade strength problem in this operation mode should be paid sufficient attention to in the design process.

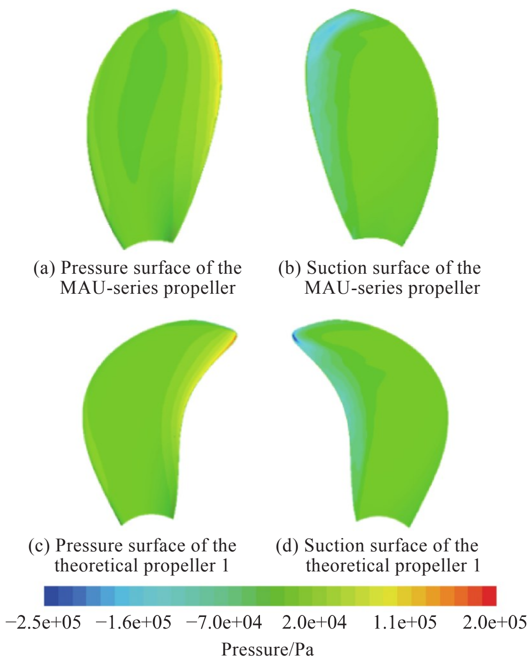

Fig. 10 Pressure distribution of blades of the two propellers in astern operation mode with $J = 0.1$

4 Influence of lift distribution coefficient on hydrodynamic performance of propeller in forward and astern operation modes

The inconsistent geometry of the two propellers is the main reason why the hydrodynamic performance of the MAU-series propeller and the theoretical propeller 1 is basically close in the forward operation mode but differs greatly in the astern operation mode.

On the basis of the design input of the theoretical propeller 1 and the requirement that the thrust in the designed forward operation mode with $J = 0.430\ 8$ is equivalent to that of the theoretical propeller 1, two theoretical propellers with zero camber or negative camber are designed by reducing the lift distribution coefficient of blade sections (denoted as the theoretical propeller 2 and theoretical propeller 3, respectively). Then, the hydrodynamic performance of the two propellers in forward and astern operation modes is numerically calculated and compared with that of the theoretical propeller 1 to further discuss the influence of the sectional lift distribution coefficient and pitch and camber combinations on the hydrodynamic performance in both operation modes.

Fig. 11 shows the radial distribution curves of the sectional lift distribution coefficients of three theoretical propellers. Figs. 12 and 13 demonstrate the radial distribution curves of the pitch ratio and camber-chord length ratio of the three theoretical propellers. It can be seen that when the theoretical propeller 1 has the largest sectional lift distribution coefficient in design, it has a large pitch ratio and a small camber. In the design of the theoretical propeller 2, the sectional lift distribution coefficient is close to 0, and the corresponding pitch increases while the camber decreases to about 0. In the design of the theoretical propeller 3, the sectional lift distribution coefficient is negative, and the corresponding camber of the propeller is also negative, while the pitch ratio increases to the maximum.

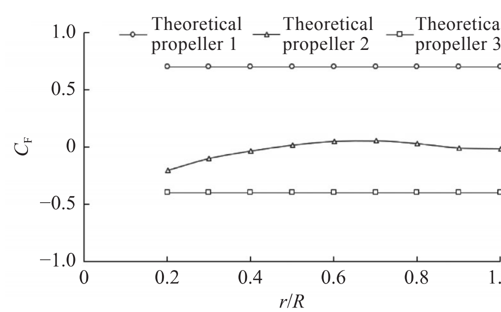

Fig. 11 Radial distribution curves of sectional lift distribution coefficients for three theoretical propellers

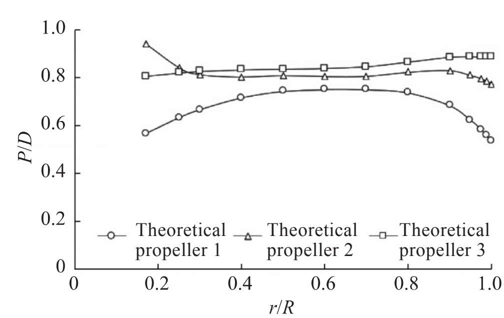

Fig. 12 Radial pitch ratio distribution of three theoretical propellers

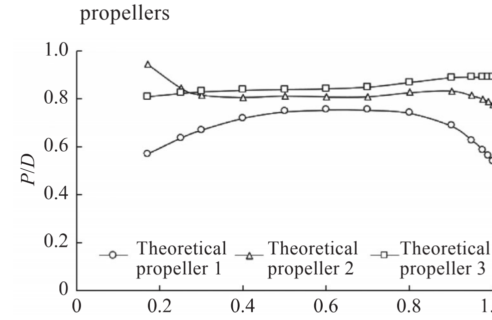

Fig. 13 Radial camber-cord length ratio distribution of three theoretical propellers

4.1 Forward operation mode

Table 4 shows the numerical calculations of the hydrodynamic performance of the three theoretical propellers in the designed forward operation mode with $J = 0.430\ 8$. Compared with the theoretical propeller 1, the theoretical propellers 2 and 3 have basically the same thrust in the designed operation mode, but the torque shows a significant increase, which results in a decrease in the open water efficiency by 5.6% and 8.9%, respectively.

Table 4 Hydrodynamic performance of three theoretical propellers under design conditions

	J	K_T	$10K_Q$	η_0
Theoretical propeller 1	0.430 8	0.170 7	0.226 6	0.516 4
Theoretical propeller 2	0.430 8	0.171 9	0.236 7	0.497 9
Theoretical propeller 3	0.430 8	0.169 5	0.247 1	0.470 3

Fig. 14 presents the pressure distribution on the blades of the three propellers in the designed forward operation mode. It can be seen that the peak pressure of the propeller near the leading edge increases significantly with the increase in the pitch ratio and the decrease in the camber ratio. The area of high pressure near the trailing edge of the blade-face pressure surface gradually decreases, while the area of low pressure near the leading edge of the blade-back suction surface gradually rises, which indicates that the contribution of the suction surface to the thrust gradually grows. The thrust contribution ratios of the blade back and face of the three theoretical propellers given in Table 5 also prove this.

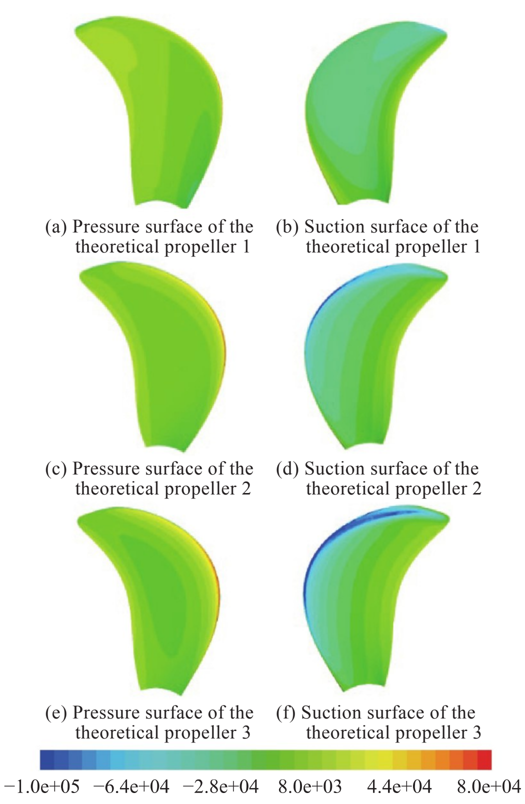

Fig. 14 Pressure distribution on blades of the three theoretical propellers in forward operation mode with $J = 0.430\ 8$

Table 5 Thrust contribution of blade back and face of three theoretical propellers under design condition

	Thrust contribution ratio/%	
	Blade-face pressure surface	Blade-back suction surface
Theoretical propeller 1	8.58	91.42
Theoretical propeller 2	6.79	93.21
Theoretical propeller 3	2.71	97.79

The above results indicate that the theoretical propeller 3 designed by the minimum lift distribution coefficient has the lowest open water efficiency and the lowest low-pressure amplitude of the blade suction surface in the forward operation mode, and the corresponding cavitation risk is the highest.

4.2 Astern operation mode

Figs. 15 and 16 demonstrate the thrust coefficient and torque coefficient curves of three theoretical propellers in the astern operation mode, respectively. It can be seen that the load of the theoretical propellers 2 and 3 is significantly increased compared to that of the theoretical propeller 1 in the astern operation mode. The average increments in thrust coefficients of the two propellers are about 34% and 51%, respectively, in the range of the operation mode discussed, and the average increments in torque coefficients of the two propellers are about 26% and 41%, respectively. The open water efficiency of the two propellers is also improved. Taking $J = 0.1$ as an example, the open water efficiency of the theoretical propellers 2 and 3 is raised by

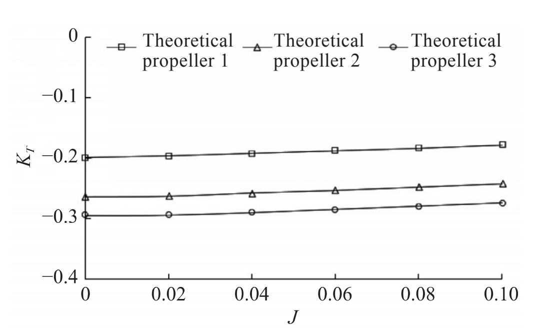

Fig. 15 Thrust coefficient curves of three theoretical propellers in astern operation mode

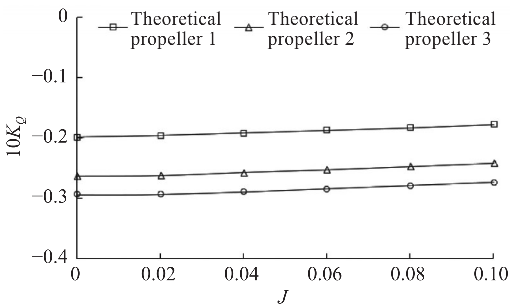

Fig. 16 Torque coefficient curves of three theoretical propellers in astern operation mode

7.4% and 8.6% compared to that of the theoretical propeller 1, respectively.

Fig. 17 shows the distribution of blade pressure of the three theoretical propellers in the astern operation mode with $J = 0.1$. It can be seen that with the rise in the pitch ratio and the drop in the camber-chord length ratio, the peak areas of the blade pressure surface of high pressure and the suction surface of low pressure gradually extend from the outer radius of the leading edge to the middle position of the chord length of the inner radius; the coverage area increases gradually, and the hydrodynamic load grows accordingly.

By comparing and analyzing the velocity triangles of typical blade sections in forward and astern operation modes, we can thoroughly analyze the reasons for the differences in the hydrodynamic performance of the three theoretical propellers. Fig. 18 shows the sectional velocity triangles of the propeller at 0.7R in different operation modes, where V_A is the advance velocity; $2\pi rn$ is the circumferential velocity; V_R is the relative inflow velocity of blade sections regardless of the induced velocity; α_k is the zero-lift angle of attack, reflecting the contribution of camber to lift; α_0 is the geometrical angle of attack, reflecting the contribution of the pitch to lift, and α is the absolute angle of attack, which is the sum of α_k and α_0. The subscripts 1, 2, and 3 represent the three theoretical propellers, respectively.

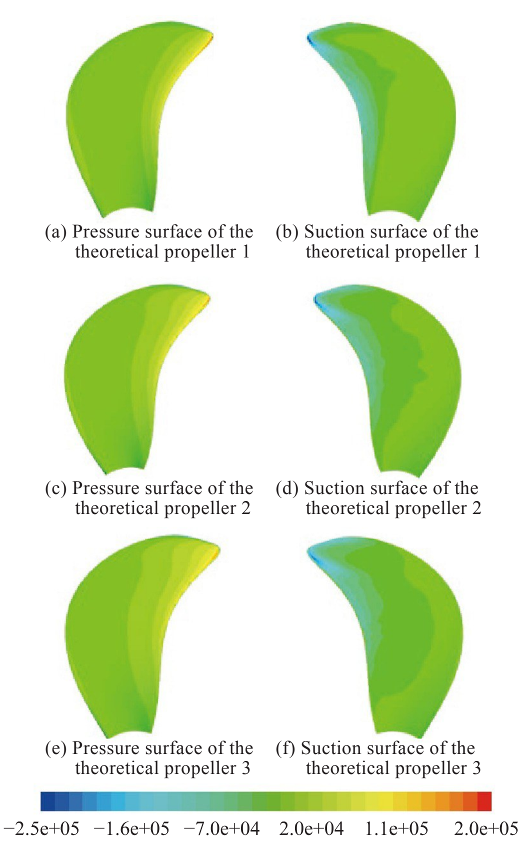

Fig. 17 Blade pressure distribution of three theoretical propellers in astern operation mode with $J = 0.1$

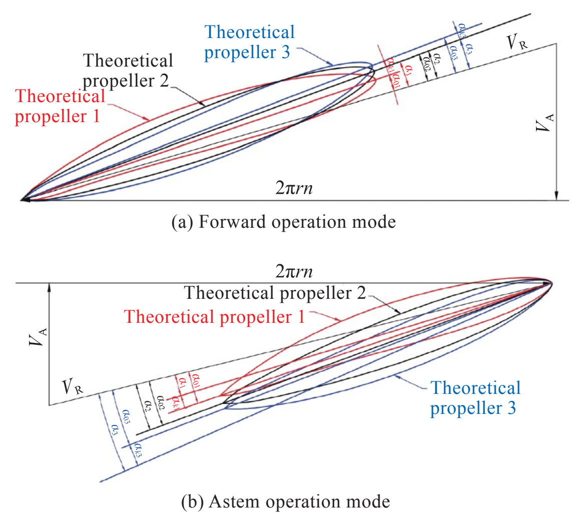

Fig. 18 Sectional velocity triangles of three theoretical propellers at 0.7R

It can be seen from Fig. 18 that the pitches of the three propellers increase in turn, and the geometrical angle of attack α_0 rises in turn in both forward and astern operation modes, namely that $\alpha_{01} < \alpha_{02} < \alpha_{03}$ always holds. In the forward operation mode, the camber of the theoretical propeller 1 is positive ($\alpha_{k1} > 0$); the camber of the theoretical propeller 2 is 0 ($\alpha_{k2} = 0$), and that of the theoretical propeller 3 is negative ($\alpha_{k3} < 0$), which eventually leads to $\alpha_1 \approx \alpha_2 \approx \alpha_3$, and their loads are basically the same. In the astern operation mode, the relative inflow is opposite, and the positions of the blade back and blade face are exchanged. The camber of the theoretical propeller 1 turns from positive to negative ($\alpha_{k1} < 0$) while that of the theoretical propeller 3 turns from negative to positive ($\alpha_{k3} > 0$), which eventually leads to $\alpha_1 < \alpha_2 < \alpha_3$. At this time, the load of the theoretical propeller 1 is the smallest, followed by the theoretical propeller 2 and theoretical propeller

3.

The above research results reveal that when the hydrodynamic performance of a propeller in the forward operation mode is not affected much, the reverse thrust of the propeller can be significantly improved by adjusting the lift distribution coefficient and changing the pitch and camber combinations of blade sections. For the ship that requires the trade-off of the forward and reverse thrusts of the propeller, in the design process of its propeller, it is recommended to select a relatively small lift distribution coefficient and minimize the influence of the camber on the lift in the forward operation mode, which is conducive to promoting the thrust performance in the astern operation mode.

5 Conclusions

In view of the engineering phenomenon that the reverse thrust of a 33 000 DWT oil product tanker with the theoretical propeller is lower than that with the MAU-series propeller, this paper first numerically calculated and analyzed the causes by the CFD method and then obtained another two schemes for the propeller by adjusting the design parameters of the propeller. The hydrodynamic performance of different propellers in forward and astern operation modes was calculated and compared, and the influence of the geometrical parameter combinations of the propeller on its performance in both operation modes was discussed. The following conclusions are drawn.

1) In both forward and astern operation modes, the propeller load decreases with the increase in the advance coefficient.

2) In forward and astern operation modes, the pitch of blade sections will generate positive lift, whereas the camber of blade sections will generate positive and negative lift alternately. The change in pitch and camber combinations of blade sections has a significant influence on the hydrodynamic performance of the propeller in forward and astern operation modes.

3) Comparatively speaking, when the hydrodynamic performance of the propeller in the forward operation mode is not affected much, adopting a large lift distribution coefficient to obtain the design scheme of a small pitch and a positive camber is conducive to improving the open water efficiency in the forward operation mode of the propeller, but is unfavorable to its reverse thrust. On the contrary, adopting a smaller lift distribution coefficient to obtain the design result of a large pitch and a negative camber will bring down the open water efficiency but raise the reverse thrust significantly.

4) In the design process of the propeller that focuses on the astern performance of the propeller, the problem of blade strength in the astern operation mode and the problem of cavitation risks on the suction surface caused by the scheme with a large pitch and a negative camber also require great concerns.

References

[1] HECKER R, REMMERS K. Four quadrant open-water performance of propellers 3710, 4024, 4086, 4381, 4382, 4383, 4384 and 4426 [R]. Bethesda, USA: David Taylor Naval Ship Research and Development Center, 1971: 411−417.

[2] JIANG C W, HUANG T T. Propeller hydrodynamic loads and blade stresses and deflections during backing and crashback operations [C]//Propellers/Shafting'91 Symposium. Virginia Beach, VA, USA: TRID, 1991.

[3] WANG G L. Study of propeller hydrodynamic performance under ice-propeller-flow interaction [D]. Harbin: Harbin Engineering University, 2016 (in Chinese).

[4] LAI H W. Hydrodynamic performance of propeller considering the influence of underwater robot on flow field [D]. Guangzhou: South China University of Technology, 2009 (in Chinese).

[5] CHEN B, STERN F. Computational fluid dynamics of four-quadrant marine-propulsor flow [J]. Journal of Ship Research, 1999, 43 (4): 218−228.

[6] CHEN H C, LEE S K. Time-domain simulation of fourquadrant propeller flows by a chimera moving grid approach [C]//Proceedings of the Civil Engineering in the Oceans VI. Baltimore, Maryland, USA: American Society of Civil Engineers, 2004.

[7] LEE S K. CFD simulation for propeller four-quadrant flows [C]//2006 SNAME Propeller/Shafting 2006 conference. VA, USA: ABS Technical Papers, The Society of Naval Architects and Marine Engineers (SNAME), 2006.

[8] XIAO B, FAN Z Z, SHI A G, et al. Numerical prediction of hydrodynamic performance of open-water propeller under multi-working conditions [J]. Journal of Dalian Maritime University, 2010, 36 (3): 7−10, 16 (in Chinese).

[9] LI L, LIU K, LI C, et al. The research on numerical simulation of propeller's hydrodynamic performance in four quadrants [J]. Ship Science and Technology, 2012, 34 (7): 8 – 14, 39 (in Chinese).

[10] WANG G B, XIE Y H, XU S J. Research on ducted propellers hydrodynamic performance in four quadrants [J]. Ship Engineering, 2015, 37 (10): 26−28, 53 (in Chinese).

[11] WANG G D. Investigation on the numerical simulation of propeller hydrodynamics, cavitation and noise [D]. Wuhan: Huazhong University of Science and Technology, 2013 (in Chinese).
[12] YANG Q F, WANG Y S, ZHANG Z H. Effects of skew and load on propeller non-cavitation and cavitation hydrodynamic performances [J]. Chinese Journal of Computational Mechanics, 2012, 29 (5): 765−771 (in Chinese).
[13] TAN T S. Performance prediction and theoretical design research on propeller in non-uniform flow [D]. Wuhan: Wuhan University of Technology, 2003 (in Chinese).
[14] CHEN J, ZOU Z J. LES simulations of the flow around a propeller in crash back and crash ahead [J]. Journal of Ship Mechanics, 2018, 22 (3): 296−310 (in Chinese).
[15] HE P P. Numerical research of fluid-structure-acoustics coupling characteristics of marine composite propellers [D]. Wuhan: Wuhan University of Technology, 2019 (in Chinese).

升力分配系数对螺旋桨正倒车水动力性能影响的数值分析

贺伟[1], 郭家伟[1], 胡小菲[2], 刘明静[2], 柏铁朝[2], 李子如[*1]
1 武汉理工大学 船海与能源动力工程学院, 湖北 武汉 430063
2 中国舰船研究设计中心, 湖北 武汉 430064

摘　要：［目的］基于数值模拟方法研究螺旋桨几何参数对其正倒车水动力性能的影响规律。［方法］以某 33 000 DWT 成品油轮为应用对象，采用RANS 方法并结合 Realiazable k-ε 湍流模型，对与其相匹配的 1 个图谱桨与 3 个理论桨在正车前进和倒车后退工况下的水动力性能进行数值仿真，讨论升力分配系数、螺距与拱度组合方式对螺旋桨正倒车水动力性能的影响规律。［结果］结果表明：在正车前进和倒车后退工况下，桨叶剖面螺距对剖面升力的贡献始终为正，拱度的贡献则体现为正负交替，螺旋桨设计时适当增加拱度减小螺距有利于提升其正车前进工况下的敞水效率，反之，采用大螺距小拱度则有利于增大倒车推力。［结论］基于研究结果给出了螺旋桨设计中兼顾考虑其正车和倒车性能的若干建议。

关键词：螺旋桨性能；倒车工况；正车工况；水动力性能；RANS